Acta Microscópica Vol. 10 N° 1, 37-53, 2001
ISSN 0798-4545 / Depósito legal pp. 199202ZU873

Three-dimensional Microstructure of Cerebellar Cortex

Microestructura Tridimensional de la Corteza Cerebelosa

Orlando J. Castejón* and Haydee V. Castejón

Instituto De Investigaciones Biológicas, Facultad de Medicina, Universidad del Zulia, Apartado 526. Maracaibo, Venezuela.
PHONE-FAX: 58-261-7929702. E-mail: ocastejo@cantv.net -

Abstract: Introduction. The microstructure of vertebrate cerebellar cortex has been reviewed at the light of information provided by comparative studies of Golgi light, confocal laser scanning, scanning and transmission electron microscopy. Material and Methods. The three-dimensional cytoarchitectonic arrangement and intracortical circuits were examined in several vertebrates taking advantage of cellular tomography and z-series of optodigital images of confocal laser scanning microscopy of the three-layered structure of cerebellar cortex, depth of focus and three-dimensional secondary electron images of conventional SEM and high resolution field emission SEM. Results. Confocal microscopy offered new information on intracortical circuits formed by mossy and climbing fibers. Scanning electron microscopy by means of cryofracture method and freeze-etching replicas for TEM provided new images on hidden outer and inner surfaces of fractured cerebellar neurons. Conventional and high resolution SEM permitted to obtain a three-dimensional image of cytoarchitectonic arrangement of cerebellar neurons and of intracortical circuits established by afferent mossy and climbing fibers and of intrinsic cortical circuits formed by cerebellar neurons. Field emission high resolution SEM offered new vistas of synaptic morphology, resolved the synaptic membrane complex and imaged the postsynaptic receptors and/or postsynaptic membrane proteins. Conclusion. The application of these integrated microscopy approaches has been extremely important for new interpretations on cerebellar structural organization and information processing.

Key words: Cerebellum, mossy fibers, climbing fibers, cerebellar neurons, correlative microscopy

Resumen: Introducción. Se revisó la microestructura de la corteza cerebelosa de los vertebrados según la información provista por estudios comparativos de microscopia de Golgi, confocal de rayos laser, electrónica de barrido y trasmisión. Materiales y Métodos: El arreglo citoarquitectónico tridimensional y los circuitos intracorticales fueron examinados en varios vertebrados mediante tomografía celular y series z de imágenes optodigitales de microscopía confocal de rayos laser de la capa triple de la corteza cerebelosa y mediante la profundidad de foco e imágenes tridimensionales de electrones secundarios de la microscopía de barrido y convencional y de emisión de campo de alta resolución. Resultados: La microscopía confocal ofreció información novedosa sobre los circuitos intracorticales formados por las fibras musgosas y trepadoras. La microscopía electrónica de barrido y el método de criofractura y la técnica de congelación-sublimación para microscopía electrónica de trasmisión proveen nuevas imágenes sobre las superficies externas e internas de neuronas fracturadas. La microscopía electrónica de barrido convencional y de alta resolución permitió obtener imagenes tridimensionales del arreglo citoarquitectónico de las neuronas cerebelosas y de los circuitos intracorticales establecidos por fibras musgosas y trepadoras y de los circuitos intrínsecos formados por las neuronas cerebelosas. La microscopía de barrido de alta resolución del tipo de emi-

Received: June, 5 2001; accepted: July, 9 2001.

Corresponding author.

sión de campo ofreció una nueva visión de la morfología sináptica, resolvió el complejo membranoso sináptico y caracterizó receptores y/o proteinas postsinápticas. Conclusión: La aplicación de un enfoque microscópico integrado es extremadamente importante para nuevas interpretaciones sobre la organización estructural y los procesos de información cerebelosos.

Palabras clave: Cerebelo, fibres musgosas, fibras trepadoras, neuronas cerebelosas, microscopía correlativa

INTRODUCTION

The three-dimensional organization of nerve cells has been mainly approached through the laborious reconstruction techniques of light and transmission electron microscopic serial sectioning, isolation of individual neurons, tissue culture, neurohistological techniques (particularly the Golgi method), intracellular staining, computer microscopy assisted methods, scanning electron microscopy, confocal scanning laser microscopy and modern optical microscopic techniques.

In the present review we report the three-dimensional microstructure of cerebellar cortex as revealed by Golgi light microscopy (GLM), confocal laser scanning microscopy (CLSM), conventional scanning electron microscopy (CSEM), high resolution scanning electron microscopy (HRSEM) and transmission electron microscopy by means of freeze-etching replica technique (FERTEM).

Cerebellar white matter

In the white matter of the teleostean cerebelli examined by light microscopy, bundles of myelinated axons, formed by afferent fibers (climbing and mossy fibers) and the efferent Purkinje cell axons have been found. In rat cerebellar folia examined by SEM at very low magnifiction, in a plane parallel to their main longitudinal axis, cerebellar afferent fibers appeared running longitudinally following the main axis of white matter (Fig. 1). The mossy fibers appear as thick fibers with a characteristic bifurcation pattern, whereas the climbing fibers are characterized as thin fibers with a typical crossing-over branching pattern. In semithin sections examined with (S) TEM, the afferent fibers appear at the entry of granule cell layer as a compact bundle of intimately apposed myelinated axons (Fig. 2), intercalated among granule cells (1).

Cerebellar Gray Matter

Light microscope and CSEM examinations of vertebrate cerebellar gray matter reveal a three layered structure: granular, Purkinje and molecular layers, Fig. 3. This regular histological organization, apparent simplicity and beautiful geometrical arrangement is extraordinarily well suited for comparative three-dimensional studies with modern optical and electron microscopy techniques.

Granule cell layer

In this layer the granule cell features, mossy fiber glomerulus and Golgi cell organization are described.

Granule cells

Earlier LM and TEM studies of cerebellar cortex (2-7) have described their basic morphological features, neuronal geometry and synaptic relationships with afferent and intrinsic fibers of cerebellar cortex. By means of CLSM the cerebellar granular layer (Fig. 4), has been explored in the x and z planes (8). Transversal and longitudinal optodigital sections were examined due to the cellular tomography of cerebellar cortex. With the FM4-64 fluorescent stain we distinguished small, medium and large granule cells, ranging from 3 to 10 μm in diameter (9). Montages of z-series of optodigital sections examined in a high performance computer equipped with MetaMorph Imaging System allowed us to estimate a granule cell/Golgi cell ratio of 50/4. Ultrathin sections and freeze-etching replicas of mouse cerebellar granule cell clusters permitted to observe their compact arrangement.

Conventional SEM and field emission SEM showed in addition the nuclear and cytoplasmic compartments of granule cells (9). The nucleus exhibits a high mass density peripheral heterochromatin and a less dense euchromatin substance. The ER appears as an interconnected trabecular system extended between the nuclear envelope and the plasma membrane (Fig. 5). Conventional SEM by means of slicing technique displayed the triangular axon hillock region of the ascending granule cell axons (10). These axons were traced throughout the granular (Fig. 6), Purkinje cell and molecular layers. The granule cell dendritic processes are also observed spreading in all directions in the granular layer and making synaptic connections with afferent mossy and climbing fibers and Golgi cell axonal ramifications. The dendrites could be traced following a twisted or convoluted trajectory up to 10 μm in length, to reach neighboring mossy and climbing fibers. The granule cell dendrites are also seen establishing synaptic contacts with afferent climbing fibers (Fig. 7). Climbing fibers are observed thinner than mossy fibers and do not form axonal expansions. They bifurcate in a cross-over manner in numerous fine, tendril collaterals that spread in all directions in the granular layer (Fig. 8). Some granule cell dendrites bifurcate also at the end of their course making synaptic con-

tacts with different climbing fiber collaterals. In addition, some short granule cell dendrites are observed establishing one to one synaptic contacts with the short beaded axonal ramifications of Golgi cells

Unipolar brush cells

These cells described by Mugnaini et al. (11, 12), to the best of our knowledge have not been studied until now with three-dimensional microscopic methods.

Golgi Cells

The larger stellate cells of the cerebellar granular layer or Golgi cells have been extensively studied at LM by Golgi, Retzius, Van Gehuchten, Kolliker and Ramón y Cajal (13). Further LM, TEM and SEM studies have been carried out among others by Fox (3) and Fox et al. (4), Eccles et al. (5), Mugnaini (6), Palay and Chan-Palay (7), Castejón and Castejón (14), Alvarez Otero and Anadon (15). In semithin sections examined by (S)TEM, the Golgi cell appears as a macroneuron intercalated among granule cell groups (Fig. 9). The GLM, CLSM and CSEM showed that the Golgi cell exhibits ascending dendrites directed toward the molecular layer and horizontal dendrites, and an axonal arborization dispersed in the granular layer, supporting former classical descriptions of these cells. At higher magnification, the axonal plexus of Golgi cells shows a typical beaded shape.

The SEM image of the large Golgi cells was comparatively similar to that obtained with the GLM. The cryofracture process with liquid nitrogen (slow freezing) exposed not only the outer surface of its cell body but in addition its dendritic and axonal ramifications (Fig. 10). The freeze-fracture method for SEM, using Freon 22 cooled by liquid nitrogen (fast freezing) revealed the fractured Golgi and granule cells. The outer surface and stereospatial arrangement of the Golgi cell RER, cellular organelles such as Golgi complex, and the nuclear chromatin were seen. In teleost fish cerebelli processed according to the freeze-fracture method for SEM, the Golgi axonal endings were observed making one to one axodendritic contacts with granule cell dendritic claws. Examination of z-series of confocal laser scanning microscopy permitted to observe numerous afferent fibers surrounding the Golgi cell soma, suggesting the high degree of information processing by Golgi cells (Fig. 11).

Mossy fiber glomeruli

The examination of the granular layer in the x and z axis with the CLSM and the study of optodigital sections using montages of z-series obtained by computer manipulation of MetaMorph Imaging System, allowed us (8, 16) to establish that about 55 to 60 granule cells and 5 to 6 Golgi cells appear surrounding each mossy glomerular region. In z-series taken at higher magnification, up to three axonal branches belonging to both, mossy and climbing fibers, were also observed in the close neighborhood of granule and Golgi cell soma. The cellular tomography at the periphery of Golgi cell soma revealed that these collateral fibers form a pericellular network. Close examination by (S)TEM, using semithin sections, showed large rosette formations of mossy fibers indented among several granule cell groups (Fig. 12). Scanning electron microscopy by means of slicing technique showed also the "en passant" synaptic contacts of mossy fibers with successive granule cell groups (Fig. 13). With the freeze-fracture method for SEM (15) an "en face view" of the internal structure of mossy glomeruli was obtained (Fig. 14). The mossy fiber rosette appears in the center surrounded by up to 18 granule cells. The granule cell dendrites were traced in a radial orientation converging upon the outer surface of the mossy fiber rosette. This SEM image offers the real image of quantitative divergence of information of nerve impulse from one mossy fiber to numerous granule cells.

Lugaro cells

In 1959, Fox (17) described Lugaro cells as a spindle shape cell transversely oriented in the granular layer and located immediately beneath the Purkinje cell layer. He described their horizontally directed dendrites in connection with the basket cell descending axonal collaterals forming the pinceaux around the axon hillock region of Purkinje cell. Fox also described descending dendrites in synaptic relationship with mossy fiber rosettes at the level of mossy glomerulus and with the Golgi cell axonal ramifications. According to this author, the axonal collaterals of Lugaro cells contact the basket cell bodies in the lower molecular layer. According to Palay and Chan-Palay (7) there are two types of horizontal fusiform cells possessing different axonal pattern and distribution. One of these types gives rise to an axon directed downwards to the granular layer and reaching the white matter as described by Ramon y Cajal (2). On the other side, Laine and Axelrad (18) described Lugaro cells with axons projected to the molecular and granular layers. Melik-Musian and Fanarjan (19) described also two Lugaro cell types with fusiform and triangular cell bodies. According to these authors, Lugaro cells exhibit projection areas ranging from molecular layer to the white substance. More recently, Laine and Axelrad (20), using electronmicroscopic gold-toning procedure and post-embedding anti-GABA immunocytochemistry, demonstrated that Lugaro cell axon forms multiple symmetrical synaptic connections with basket and stellate cell soma and proximal dendrites.

Purkinje cells

Fox (3), Fox et al. (4), and Eccles et al. (5) carried out GLM and TEM studies of vertebrate Purkinje cells. The most detailed description of Purkinje cells by LM, TEM and Golgi rapid impregnation by high voltage EM has been given by Palay and Chan-Palay (7). The recurrent collaterals of Purkinje cell axons were described by Chan-Palay (21) by GLM and TEM. As classically de-

scribed, Golgi light microscopy (Fig. 15), shows a pear shaped cell soma provided with a primary dendritic trunk with secondary and tertiary dendrites in the molecular layer, which have been also clearly visualized by means of CLSM, using FM4-64 (Fig. 16).

In z-series of CLSM of hamster cerebellum, the climbing fibers have been observed (Fig. 17), approaching to the Purkinje cell soma (8). Castejón and Caraballo (22) by means of slicing techniques, Castejón and Valero (23) using ethanol cryofracturing technique, Scheibel et al. (24) by means of the creative tearing technique, Hojo (25) by means of t-butyl alcohol freeze-drying device and Arnett and Low (26) by using ultrasonic microdissection exposed at SEM level the outer surface of Purkinje cells (Fig. 18), and dendritic branchlets, the surrounding basket cell soma, axonal collaterals and segments of climbing fibers. Takahashi-Iwanaga (27) showed the reticular endings of Purkinje cell axons in the rat cerebellar nuclei by means of NaOH maceration. As classically described, the Purkinje cell surface appears partially ensheathed by the satellite Bergmann glial cells. During the SEM preparative procedures, the Bergmman glial cells are selectively removed allowing the visualization of Purkinje cell outer surface. The Purkinje cell soma exhibited a typical pyriform, flask or round shape. It was possible to obtain a view of the lower pole of Purkinje cell, the axon hillock region of Purkinje cell axon and its infraganglionic plexus. Freeze-etching replica technique for TEM shows the three-dimensional organization of nuclear and cytoplasmic compartments (Fig. 19).

The smooth ER of Purkinje cell was analyzed by Martonne et al. (28) in serial sections for TEM and semithin and thick sections for intermediate high voltage EM; it was seen forming a highly interconnected network of tubules and cisterns extended throughout the dendritic shaft and into the spines Terasaki et al. by means of confocal microscopy, using Dil as a fluorescent stain reported also a continuous compartment of ER from the cell body throughout the dendrites (29). Kanaseki et al. (30), using quick-freezing technique followed by freeze-substitution for ultrathin sectioning or freeze-fracturing and deep-etching replicas, showed that all smooth ER are rough-surfaces heavily studded with a large number of small dense projections. The localization of these projections coincides with the distribution of the inositol 1,4,5-triphosphate (IP3) receptor determined by quantitative immunogold electron microscopy. Castejón (1), using the freeze-fracture method for SEM applied to teleost fishes, showed at the longitudinal and cross sections of Purkinje secondary dendritic ramifications, the ER profiles and cytoskeletal elements forming a microtrabecular arrangement, in which cell organelles appear suspended (Fig. 20).

Molecular layer

Climbing fiber terminal collaterals were observed ending at the molecular layer (Fig. 21), in a typical cross-over or arborescence pattern type of bifurcation, characteristically spreading in three different planes (31, 32). In freeze-etching replicas for TEM they finished by means of bulbous endings applied directly upon the surface of Purkinje dendritic spines (Fig 22). An extensive contact of climbing fibers with Purkinje cells has been demonstrated by Alvarez-Otero et al. (33) in elasmobranch cerebellum using Cajal reduced silver technique, Golgi method and electron microscopy. Field emission HRSEM shows the three-dimensional shape of Purkinje spines (Fig. 23), in fractured regions where the presynaptic fibers have been removed by the cryofracture method. The spine body and neck were clearly distinguished.

The parallel fibers or granule cells axons have been also traced in the human cerebellar molecular layer processed by freeze-etching replica for TEM, CSEM and ethanol-cryofracturing technique for SEM. The parallel fiber exhibits non-synaptic segments and synaptic varicosities. In freeze-etching replicas they appear in cross-sections as a compact bundle of unmyelinated axons (Fig. 24), running perpendicular to the Purkinje cell dendritic ramifications (Fig. 25). They showed "en passant" axo-dendritic synapses with many successive Purkinje dendrites (1, 34-36) supporting former LM and TEM descriptions (7). The non-synaptic segments of parallel fibers appear as fine, high mass density threads (Fig. 26), applied tangentially to the outer surface of Purkinje dendrites. The synaptic segments or synaptic varicosities of parallel fibers have been observed by means of high voltage EM, and TEM freeze-etching replicas and SEM (7, 34, 35), intimately applied to the bulbous soma of Purkinje dendritic spines making "en passant" axospinodendritic contacts. Freeze-etching replicas of parallel fiber-Purkinje spine synapses (Fig. 27), show the aggregated intramembrane particles at the postsynaptic membranes, corresponding to the localization of postsynaptic receptors and/or postsynaptic proteins.

Field emission high resolution SEM (FEHRSEM) helped us also to elucidate parallel fiber-Purkinje spine synaptic relationship (35, 37). The use of a delicate specimen preparation procedure, the cryofracture method in Freon 22 cooled by liquid nitrogen, the use of chromium coating and the "in lens" system of field emission electron microscope permitted to obtain SE-I images. Fractured synaptic varicosities of parallel fibers showed the spheroidal synaptic vesicles and the limiting plasma membrane (Fig. 28). Fractured Purkinje spines showed the profiles of endoplasmic reticulum. Parallel fiber-Purkinje spine synaptic relationship was studied by means of FEHRSEM in Rhesus monkey cerebellar cortex, in a attempt to resolve its structure and three-dimensional organization. The parallel fiber presynaptic ending exhibited the topographic contrast of clustered spheroidal synaptic vesicles, about 50 nm in diameter, which appear surrounded by an homogeneous extravesicular material. The synaptic membrane complex (Fig. 29), showed the SE-I profile of the pre- and

postsynaptic membranes and the interposed synaptic cleft. The postsynaptic membrane and the associated postsynaptic density show a discontinuous surface formed by round subunits, 25-35 nm in diameter. By their localization, they can be correlated with postsynaptic intramembrane particles, postsynaptic proteins or neurotransmitter receptor units.

Basket cells

Cerebellar basket cells have been extensively described by GLM and TEM (2, 3, 4, 7, 38). They have a round, triangular or oval shape and are localized in the lower third of molecular layer or between the Purkinje cells. As clearly demonstrated by GLM, the axon of basket cell emerges directly either from the cell body or from one of the major dendrites. It follows an horizontal course in the parasagittal plane running through several Purkinje cells. The axon gives off three types of collaterals: a) descending collaterals that approximate in cascade over the primary dendritic trunk and cell bodies of several Purkinje cells (Fig. 30), b) ascending collaterals toward the molecular layer and c) transverse collaterals that remain in the plane of cell body and give off in turn, descending collaterals contributing to the Purkinje pericellular nest and pinceaux, and ascending collaterals also directed to the molecular layer. The capability for cellular tomography offered by CLSM allowed us to image basket cell soma (Fig. 31), and processes and to study the topographic relationship with Purkinje cells (38). The exploration of the cerebellar cortex in the x and z planes permitted to trace basket cell dendritic processes in the molecular layer, and basket axonal collaterals in the Purkinje cell layer. The basket cell dendrites were observed arising from the upper side of cell body and expanding in vertical direction toward the molecular layer, forming a fan-shaped field in the parasagittal plane. The ethanol-cryofracturing technique for SEM (Fig. 32) exposed the basket cell axonal collaterals applied to the Purkinje cell outer surface soma. The axonal descending collaterals of basket cells were observed at the level of the Purkinje cell axonal initial segment contributing to the formation of the pinceaux. Close examination of the Purkinje pericellular nest showed the basket cell endings applied to the Purkinje cell plasma membrane and containing flattened and ellipsoidal synaptic vesicles and neurofilaments (7, 38). Axosomatic synapses formed by parallel and climbing fibers were also observed upon the basket cell soma.

Stellate neurons

The short history and most complete description of these neurons has been given by Palay and Chan-Palay (7) by means of camera lucid drawings of Golgi preparations and TEM. At SEM level, superficial short-axon stellate neurons with round, elliptical or fusiform somata are observed mainly localized in the outer third molecular layer (39). Three to five beaded dendrites radiate from the cell body toward the neighbouring Purkinje dendrites or other stellate cells. The axon is originated by means of a typical triangular shaped axon hillock and, after a short initial segment, it bifurcates into tenuous varicose collaterals. Short, ramified and beaded dendrites emerge from the cell somata, directed toward the passing bundles of parallel fibers. With the freeze-etching replica technique the cytological organization of stellate neurons can be appreciated in detail (Fig. 33). With the freeze-fracture technique for SEM, the stellate neurons were fractured through the equatorial plane, showing at low magnification, a condensed pattern of nuclear heterochromatin and a thin rim of perinuclear cytoplasm. Fractured stellate neurons showed the three-dimensional image of the GERL complex, formed by the Golgi cisternae and their sacs, endoplasmic reticulum canaliculi and lysosomes. This image could be also correlated with the thin section appearance of these organelles located in the nuclear poles of stellate neurons. Paula Barbosa et al. (40), by means of a combined GLM and TEM study, showed the axonal descending branches of stellate cell forming the pericellular basket and pinceau.

Serotoninergic and catecholaminergic cerebellar afferents

In addition to the afferent mossy and climbing fibers, there are also a catecholaminergic and a serotoninergic innervation in the cerebellar cortex (41, 42). These afferent fibers have not been three-dimensionally characterized thus far.

Neuroglial cells. Bergmann glial cells

Bergmann glial cells or Golgi epithelial cells are regional types of cerebellar astrocytes firstly described by Golgi and subsequently studied at LM level by Ramón y Cajal, Terrazas and Fañanas, and Ramón y Cajal (2). An almost complete account of TEM features and stereograms of Golgi preparations taken with high voltage electron microscope has been given by Palay and Chan-Palay (7). At the LM, the Bergmann glial cells appear as round, elongated or triangular cell shaped bodies applied to the Purkinje cell soma. They exhibit a clear cytoplasm and a vesicular nucleus. The cytoplasm ensheats the Purkinje cell body surface and the axon hillock region. Their ascending processes (Bergmann fibers) are observed surrounding the Purkinje primary dendrites and accompanying the secondary and tertiary dendrites in the molecular layer. With SEM, using the freeze-fracture preparative procedure (43), the outer surface of Bergmann glial cell soma could be visualized and exposed for the first time in teleost fish cerebellar cortex and characterized by their satellite position to the Purkinje cell (Fig. 34).

The freeze-etching replicas of mouse cerebellar cortex offered a three-dimensional aspect of fractured Bergmann glial cell soma and a more accurate view of topographical relationship of Bergmann glial lamellated processes with Purkinje dendrites, parallel fibers

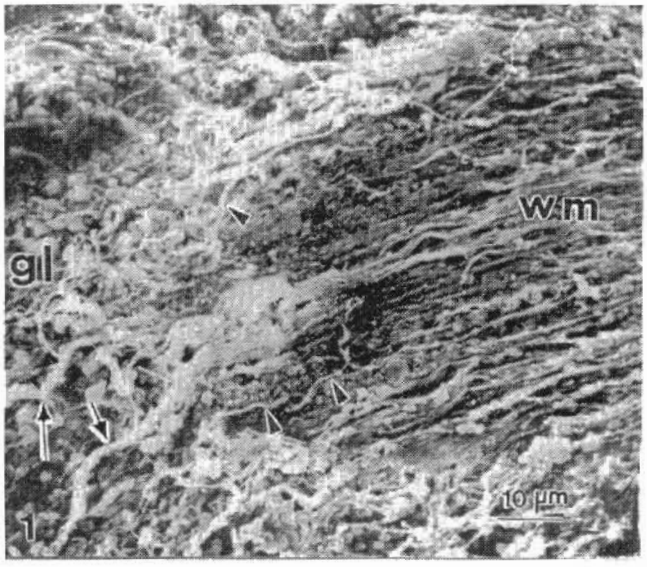

Figure 1. Conventional scanning electron micrograph of rat cerebellar cortex showing the afferent thick mossy fibers (arrows) and the thin climbing fiber (arrowheads) entering from the white matter (wm) to the granule cell layer (gl).

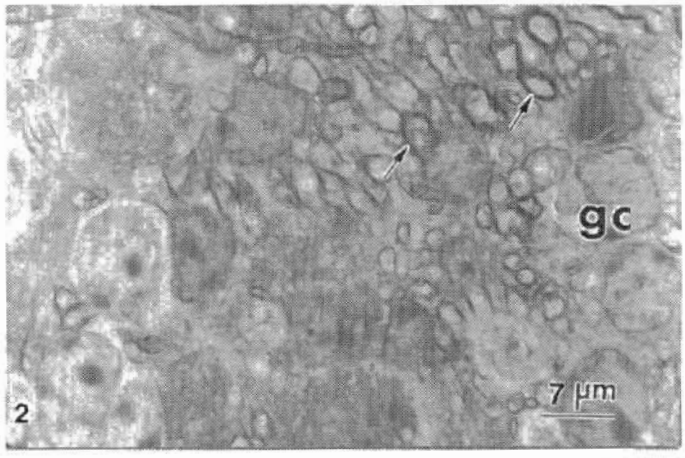

Figure 2. Scanning-transmission electron micrograph of a semithin section of mouse cerebellar granular layer showing the cross sections of myelinated afferent fibers (arrows) and the granule cells (gc).

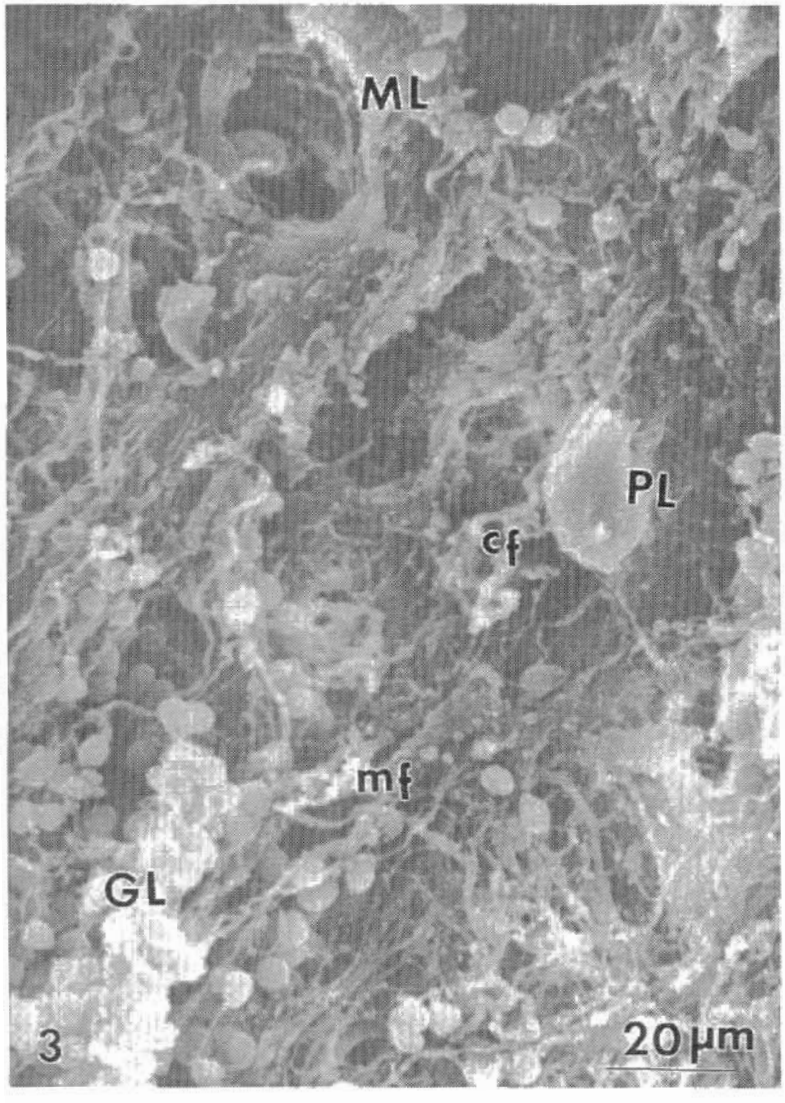

Figure 3. Conventional scanning electron micrograph of teleost fish cerebellar cortex showing its three-layered structure: granular (GL), Purkinje (PL) and molecular (ML) layers. The mossy fibers (mf) remain in the granule layer. The climbing fibers (cf) ascend to the Purkinje cell and molecular layers.

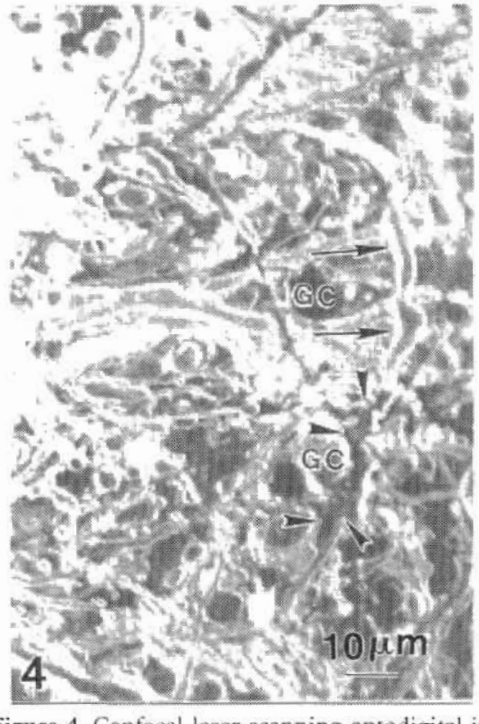

Figure 4. Confocal laser scanning optodigital image of hamster cerebellar granular layer showing the mossy fiber trajectory (arrows) and the rosette formation (arrowheads) among the granule cells (GC). With permission of Scanning.

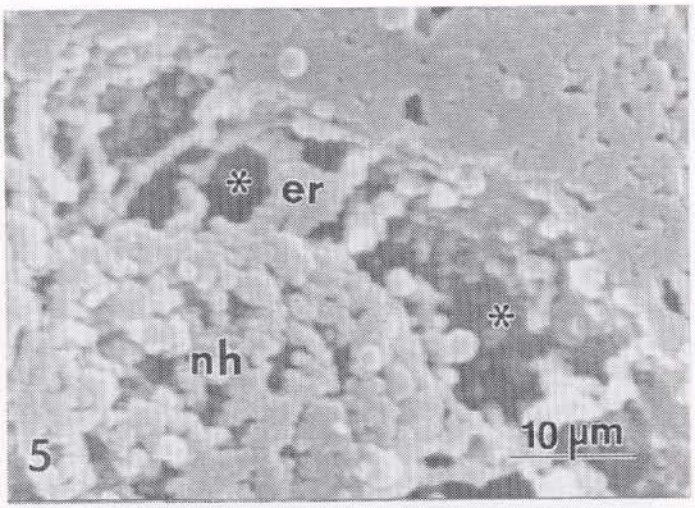

Figure 5. Scanning electron micrograph of a teleost fish fractured granule cell showing the nuclear heterochromatin (nh) and the endoplasmic reticulum canaliculi (er), extended between the nucleus and the plasma membrane. The cytosol has been washed out during the freeze-fracture SEM preparative method leaving empty dark spaces (asterisks), facilitating the visualization of inner cell

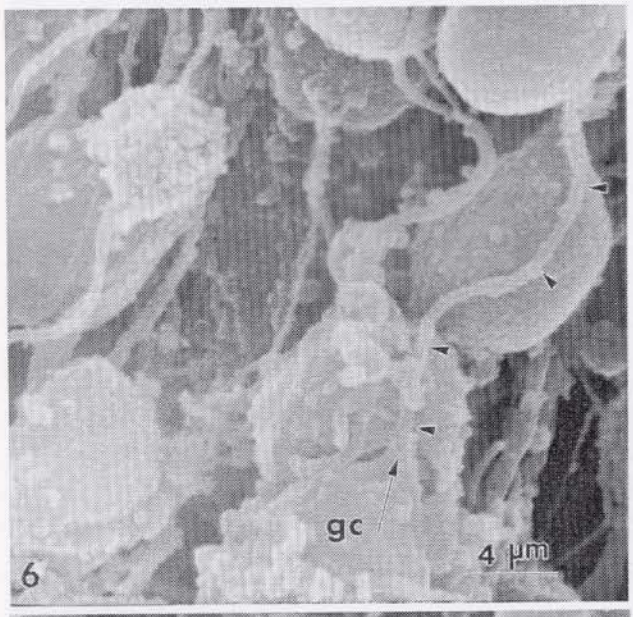

Figure 6. Teleost fish cerebellar granular layer showing the granule cell outer surface (gc), the granule cell axon hillock region (arrow) and a segment of the ascending granule cell axon (arrowheads).

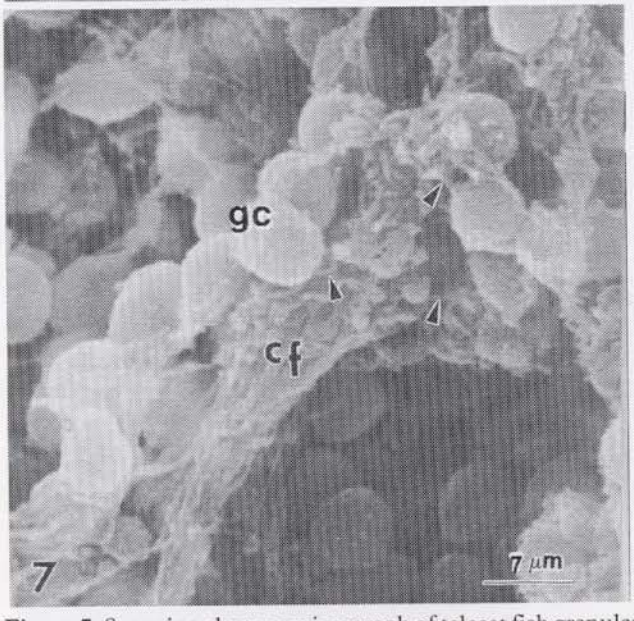

Figure 7. Scanning electron micrograph of teleost fish granular layer showing a climbing fiber bundles (cf) establishing synaptic relationship with granule cell (gc) dendrites (arrowheads). With permission of Scanning Microscopy.

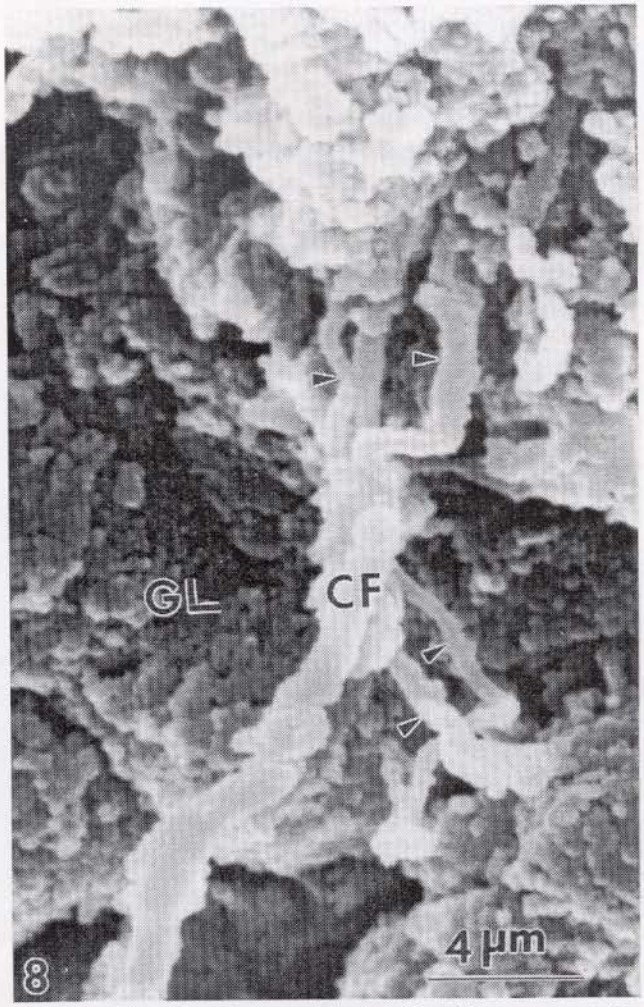

Figure 8. Scanning electron micrograph of human cerebellar granular layer showing the parent climbing fiber (CF) and their collaterals (arrowheads) in the granular layer (GL). Ethanol -cryofracturing technique. With permission of Scanning Microscopy.

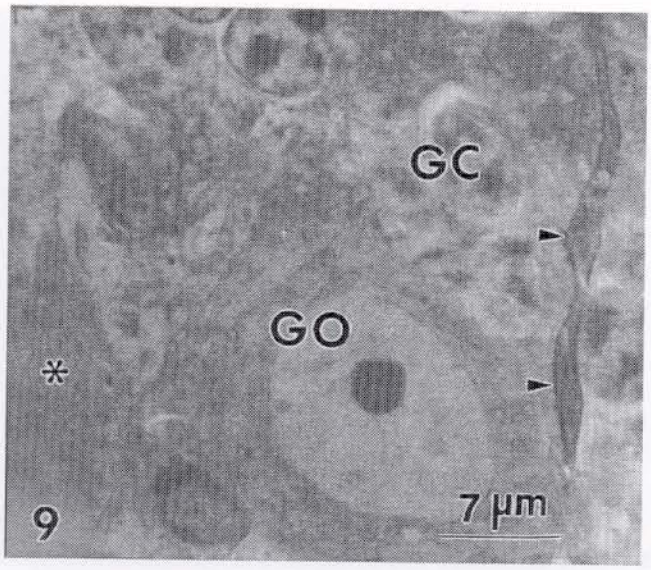

Figure 9. Scanning transmission electron micrograph of a semithin section of mouse granular layer showing the Golgi cell (GO) and the surrounding granule cells (GC). The asterisk labels the mossy glomerular region. A myelinated axon (arrowheads), presumably a climbing fiber, is also seen.

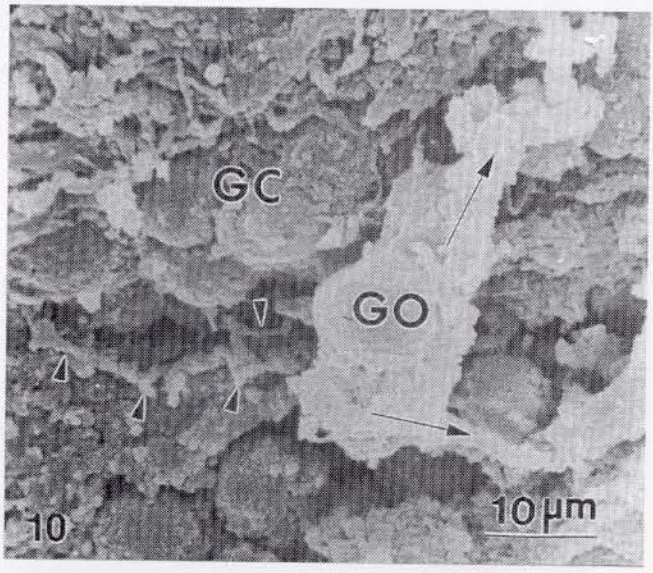

Figure 10. Scanning electron micrograph of human cerebellar granular layer displaying a Golgi cell (GO), surrounded by granule cell (GC) groups. The arrows indicate the ascending and horizontal dendrites. The axonal plexus has been labeled with arrowheads. Ethanol-cryofracturing technique.

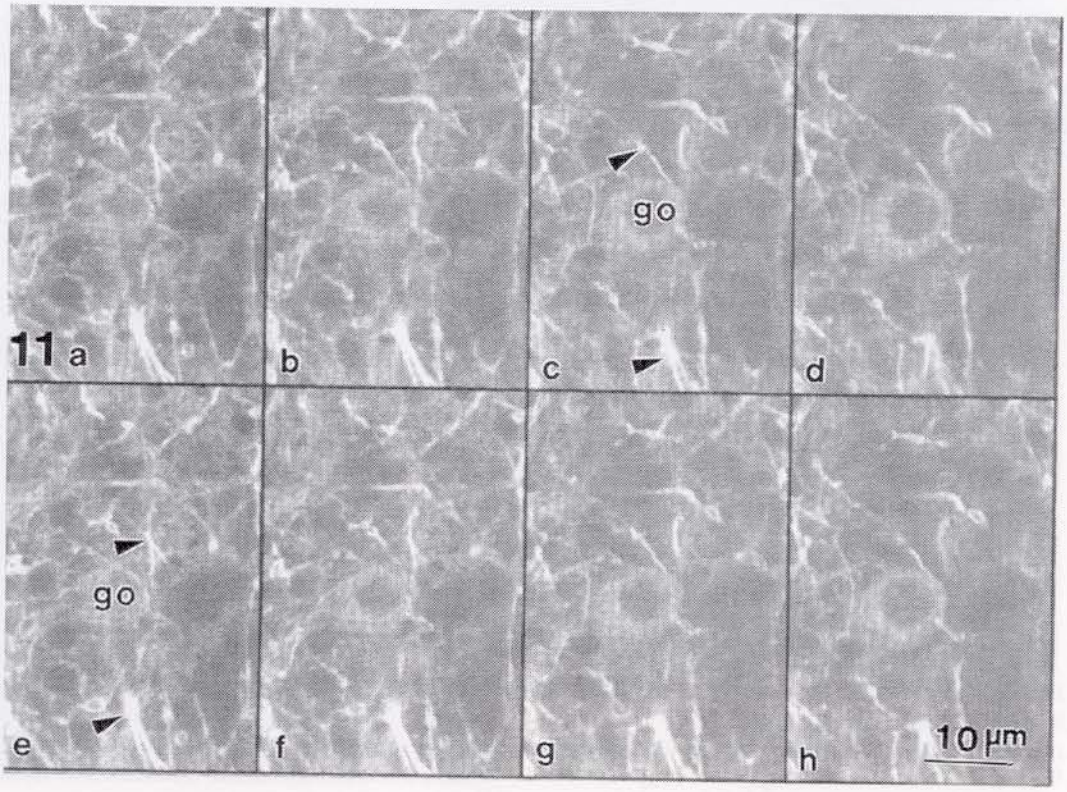

Figure 11 a-h. Confocal laser scanning microscopy of a z-series of hamster cerebellar granular layer showing the Golgi cell (go) and numerous afferent myelinated axons (arrowheads), corresponding to mossy and climbing fibers. These optodigital images show a high degree of information processing around Golgi cell.

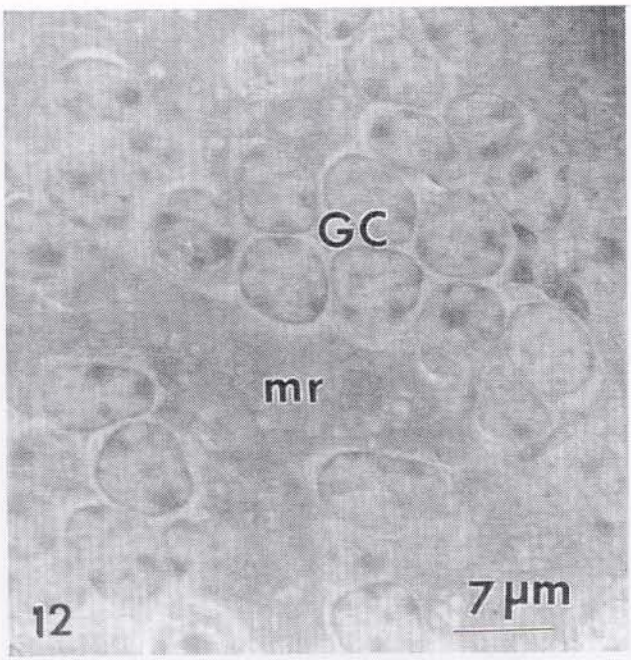

Figure 12. Scanning-transmission electron micrograph of a semithin section of mouse cerebellar cortex showing a large mossy fiber rosette (mr) intercalated among granule cell groups (GC).

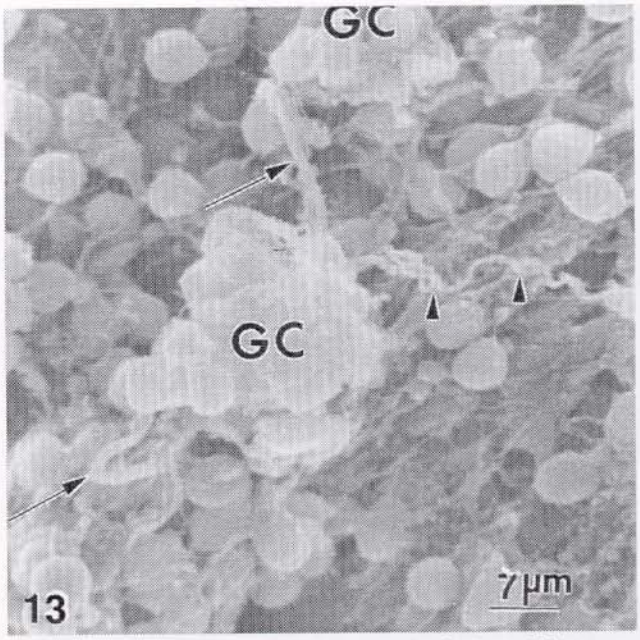

Figure 13. Scanning electron micrograph of teleost fish granular layer showing a mossy fiber (arrows) entering into two successive granule cell groups (GC) and establishing "en pasant" synaptic contacts with granule cell dendrites. The fine beaded axonal ramification of Golgi cell (arrowheads) is also observed participating in the mossy glomerular region. With permission of Scanning Microscopy.

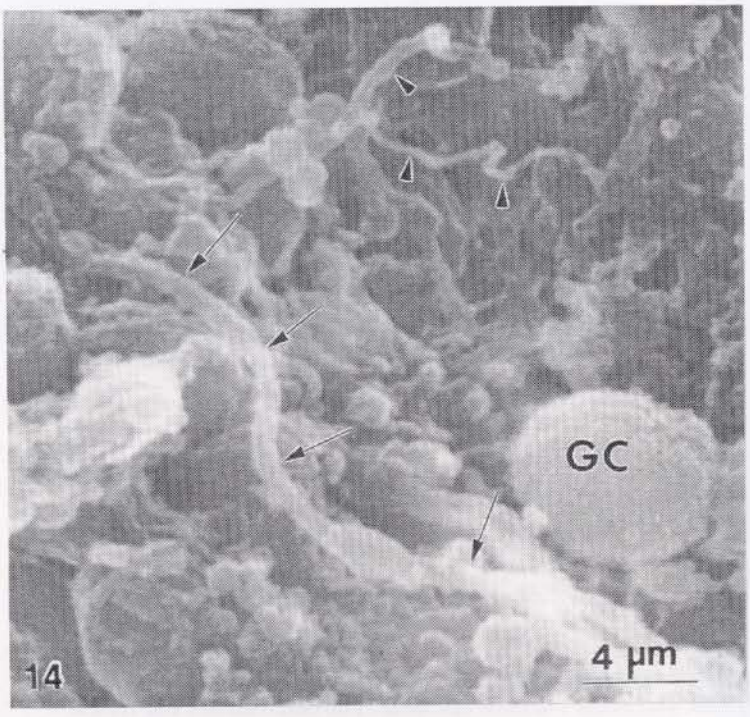

Figure 14. Scanning electron micrograph of teleost fish cerebellar fractured glomerular region showing the longitudinal course of the central mossy fiber (arrows), surrounded by the granule cell (GC) dendrites. The fine beaded axonal ramifications of Golgi cell are also seen (arrowheads). Freeze-fracture SEM method.

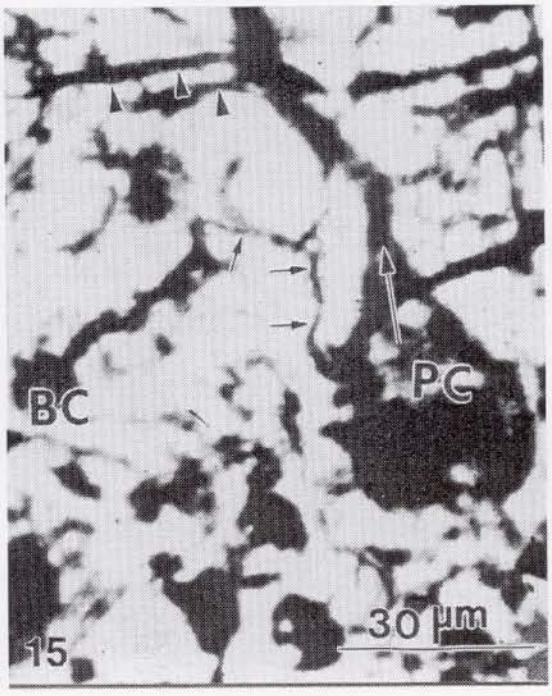

Figure 15. Golgi light photomicrograph of mouse Purkinje cell (PC) showing a pear shaped body, the primary trunk (arrow) and secondary dendritic branches (arrowheads). A descending basket cell (BC) axonal collateral (short arrows) are seen approaching to the Purkinje cell soma.

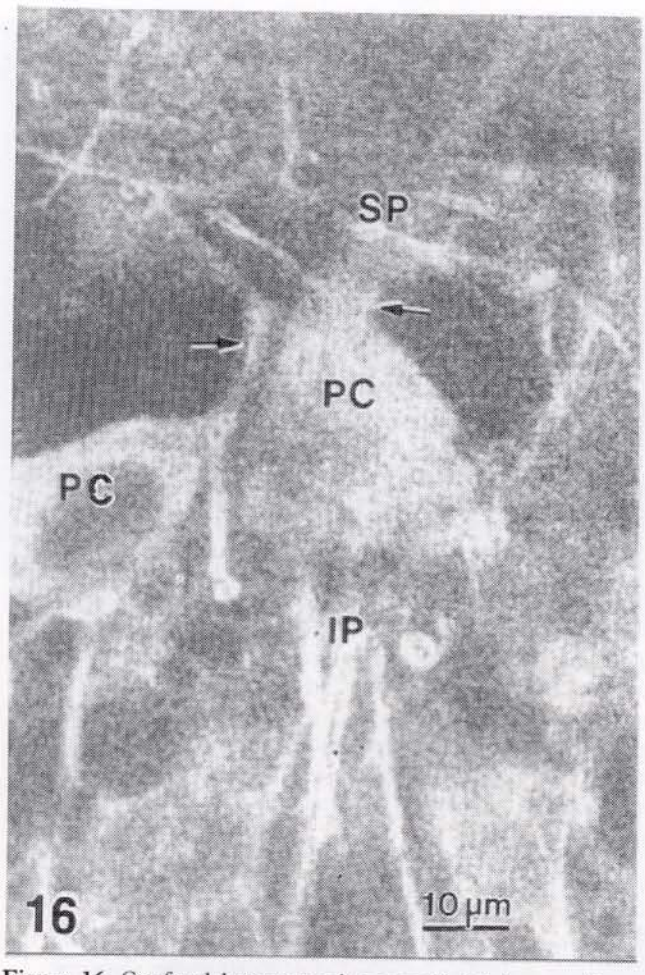

Figure 16. Confocal laser scanning optodigital image of two Purkinje cells (PC). A partial image of supraganglionic (SP) and infraganglionic (IP) plexuses is observed. The short arrows indicate the primary dendritic trunk.

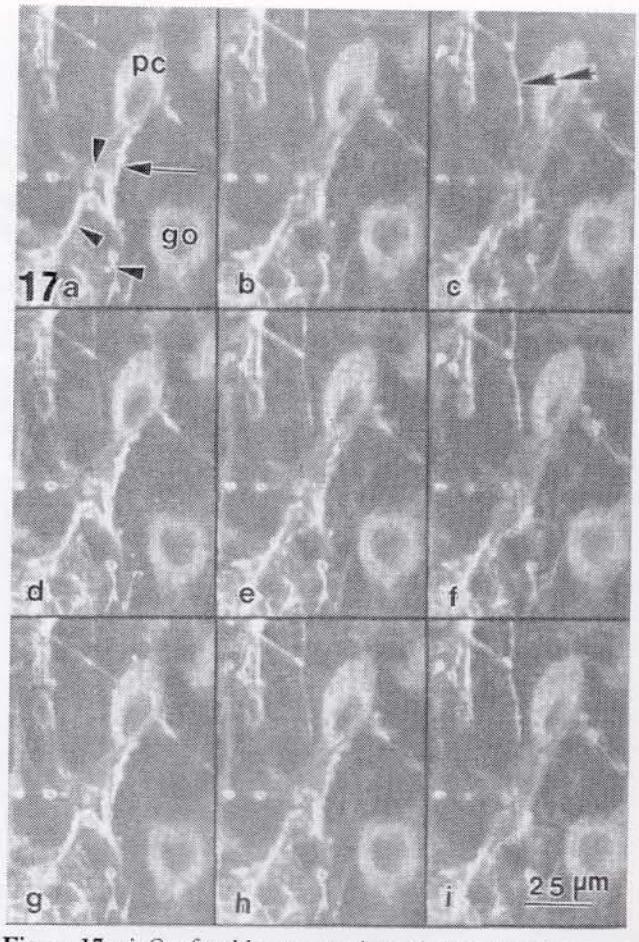

Figure 17 a-i. Confocal laser scanning microscopy of a z-series of hamster cerebellar cortex showing the climbing fiber collateral arborisation at the granular layer. Some collaterals (arrowheads) remain at the granular layer and others (arrow) ascend to the Purkinje cell soma (pc). At c, a climbing fiber ascends directly to the molecular layer (double arrowhead). A Golgi cell (go) is also seen. With permission of Biocell.

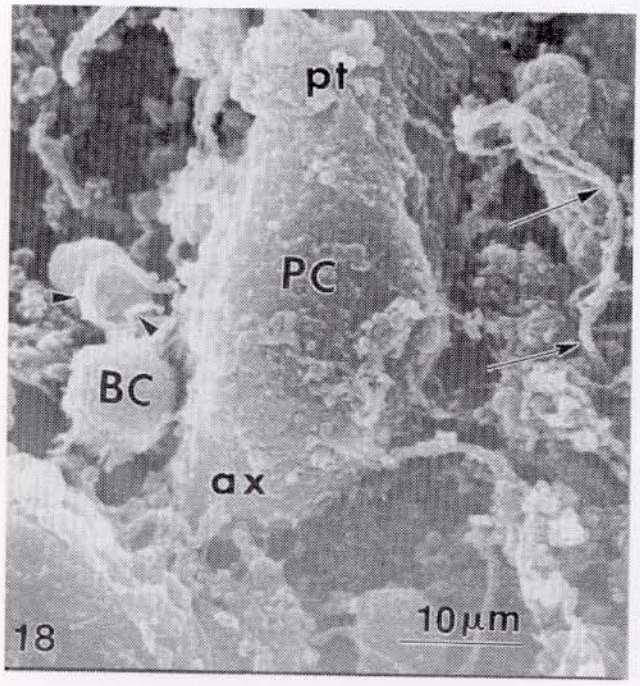

Figure 18. Scanning electron micrographs of teleost fish cerebellar Purkinje cell layer. The outer surface and typical pear shape of Purkinje cell (PC) can be observed. The enveloping Bergmann glial cell has been removed by the SEM preparative procedure. A basket cell (BC) is observed sending their processes (arrowheads) toward the Purkinje cell soma. The site of emergency of primary dendritic trunk (pt) and the axon hillock region (ax) are also seen. A climbing fiber (arrows) is observed ascending to the molecular layer.

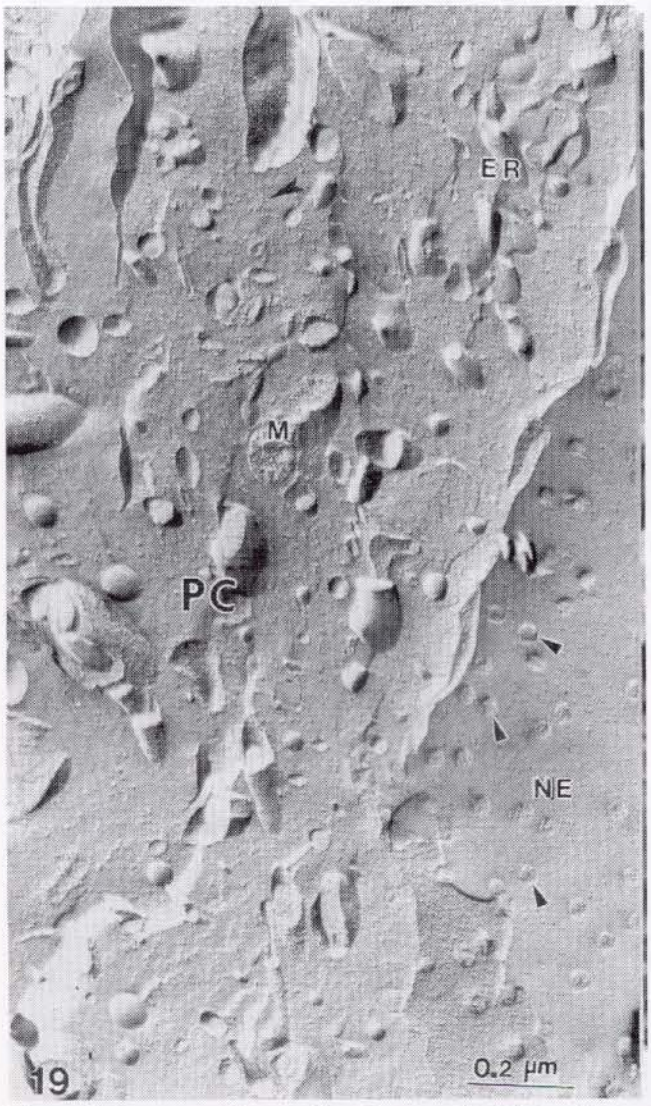

Figure 19. Freeze-etching replica of a mouse Purkinje cell cytoplasm (PC) showing the three-dimensional relief of endoplasmic reticulum (ER) profiles, mitochondria (M) and the fractured nuclear envelope (NE) showing the nuclear pores (arrowheads).

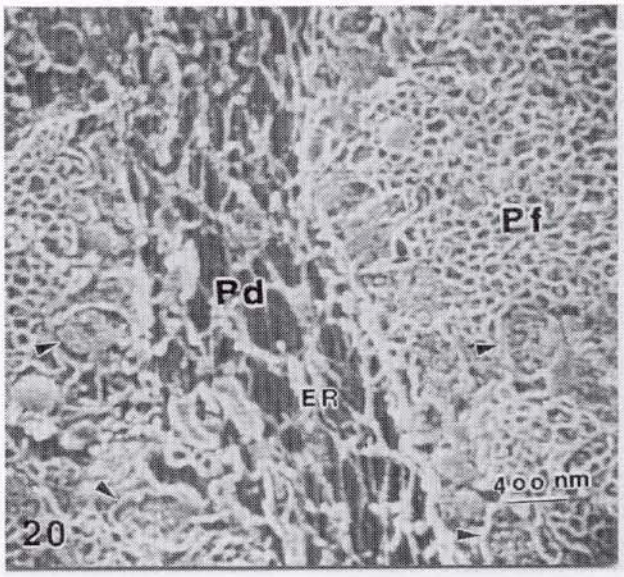

Figure 20. Scanning electron micrograph of a fractured Purkinje cell dendrite (Pd) exhibiting the trabecular arrangement of endoplasmic reticulum (ER). The cross sections of non-synaptic segments of parallel fiber bundles (Pf) are seen. The parallel fiber synaptic varicosities (arrowheads) contain spheroidal synaptic vesicles. Freeze-fracture SEM method.

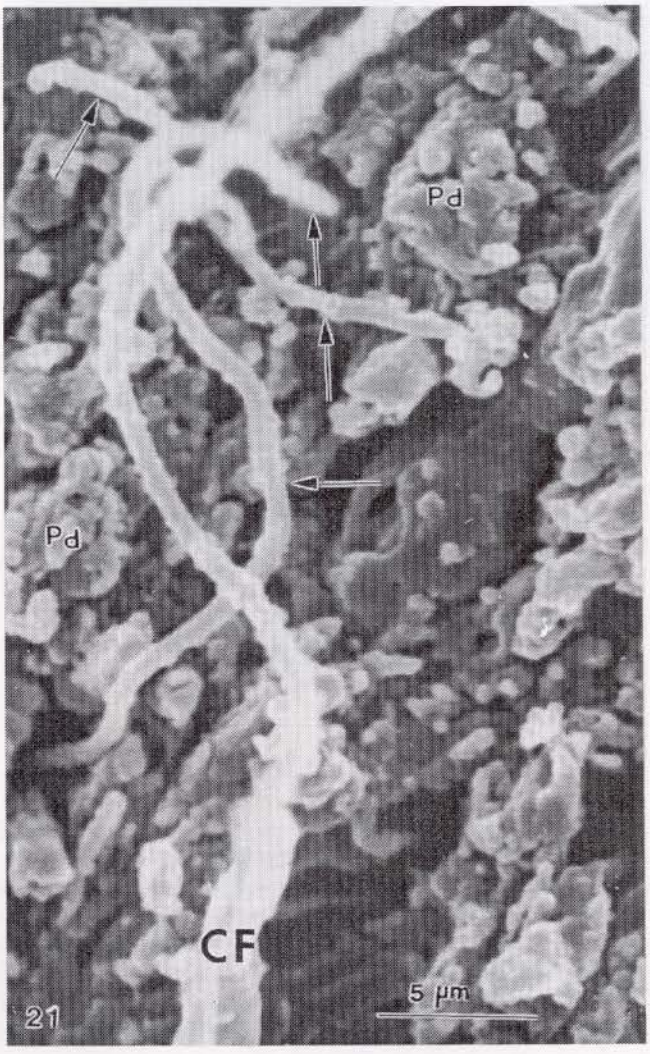

Figure 21. Scanning electron micrograph of human of cerebellar cortex showing the parent climbing (CF) fiber and their collaterals (arrows) in the molecular layer insinuating between Purkinje dendritic arborisation (Pd).

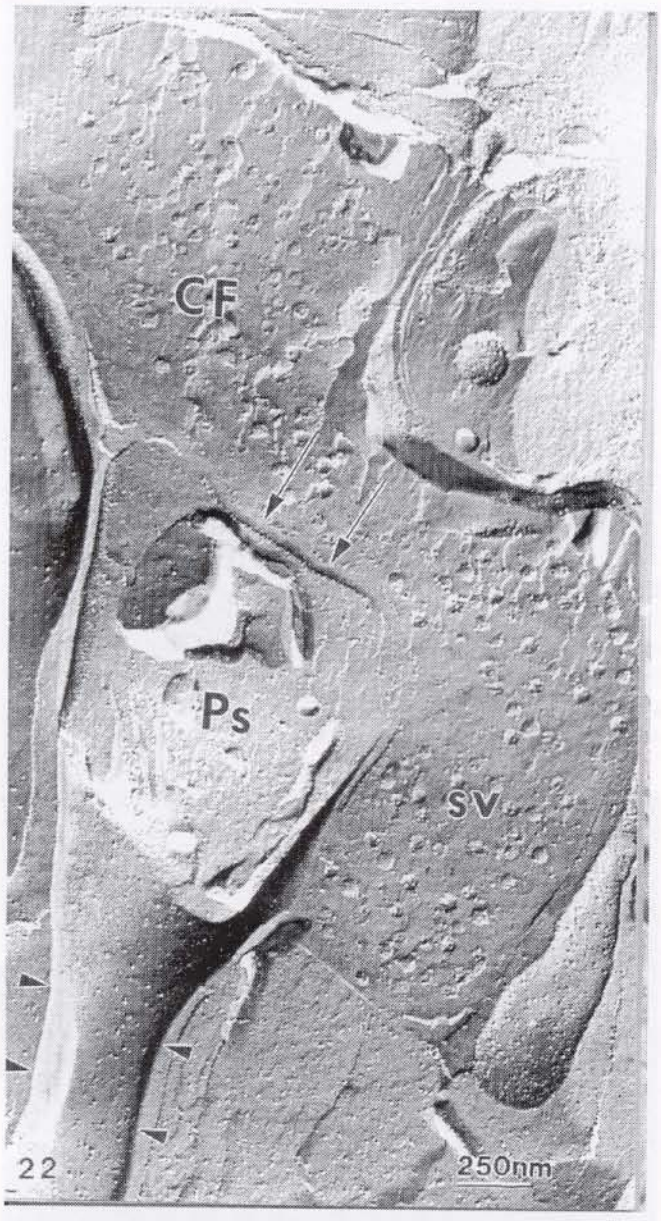

Figure 22. Freeze-etching replica of mouse cerebellar cortex showing a large climbing fiber ending (CF) containing spheroidal synaptic vesicles (sv) and establishing synaptic contact (arrows) with the body of a Purkinje dendritic spine (Ps). The arrowheads indicate the spine neck.

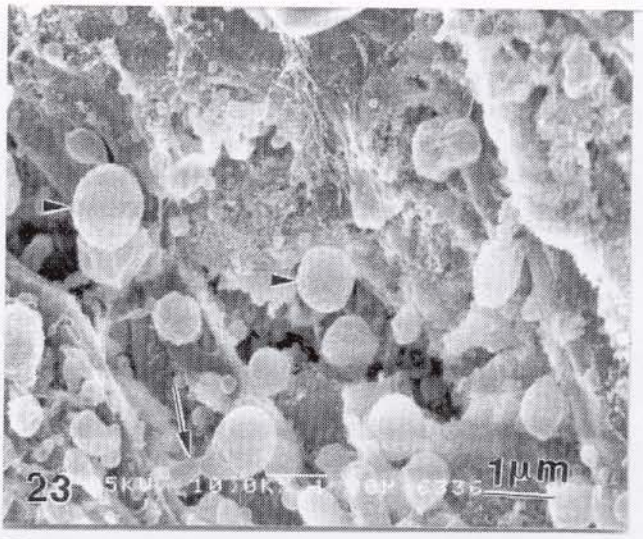

Figure 23. Field emission high resolution SEM of mouse cerebellar molecular layer showing the Purkinje dendritic spines. The presynaptic ending has been removed by the cryofractured method. Note the neck (arrow) and the body (arrowheads) of Purkinje spines.

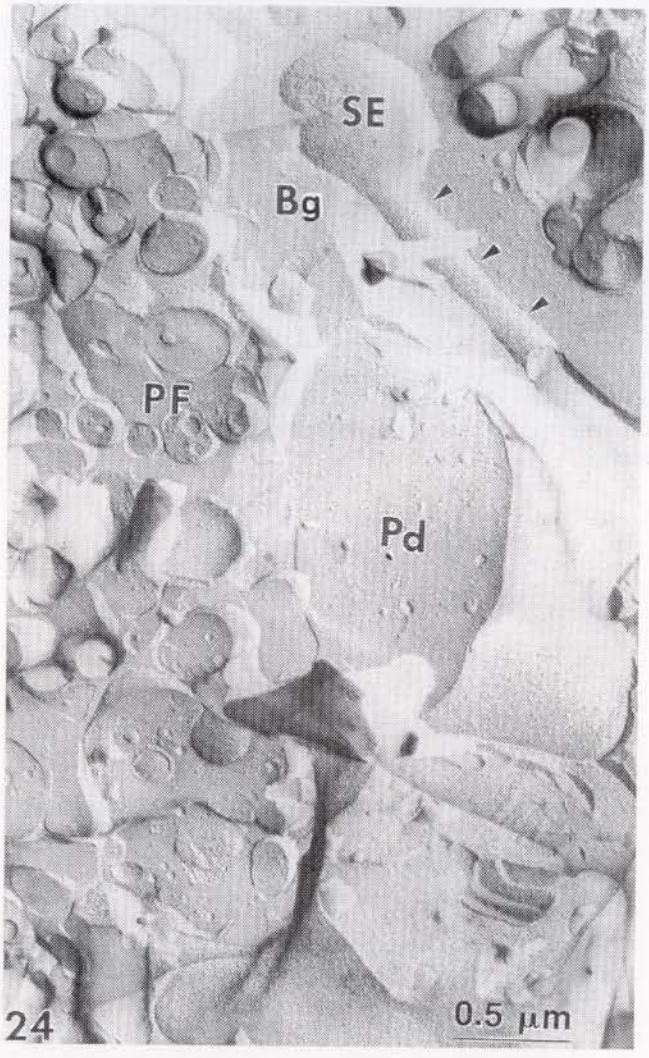

Figure 24. Freeze-etching replica of mouse cerebellar molecular layer showing the cross sections of parallel fiber bundles (PF) surrounding a Purkinje dendritic branch (Pd). A longitudinally fractured parallel fiber exhibits the nonsynaptic segment (arrowheads) and the "en pasant" synaptic ending (SE). The Bergmann glial cell cytoplasm (Bg) is also seen insulating nerve processes.

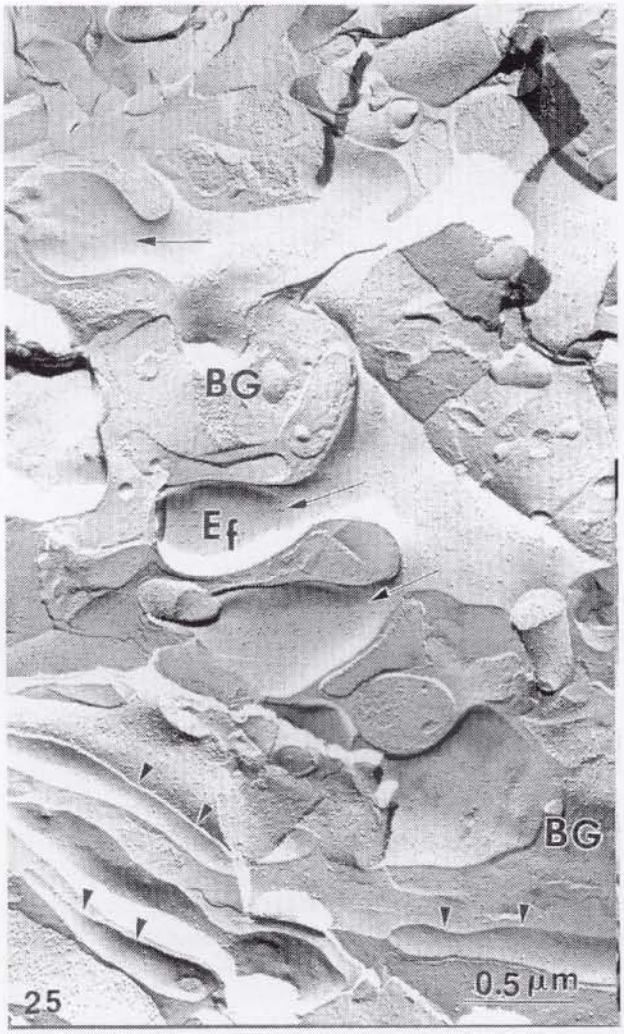

Figure 25. Freeze-etching replica of mouse cerebellar molecular layer showing the E face (Ef) of Purkinje cell dendritic spines (arrows). The longitudinal course of parallel fibers (arrowheads) is also seen. The Bergmann glial cell cytoplasm (BG) appears enveloping both structures.

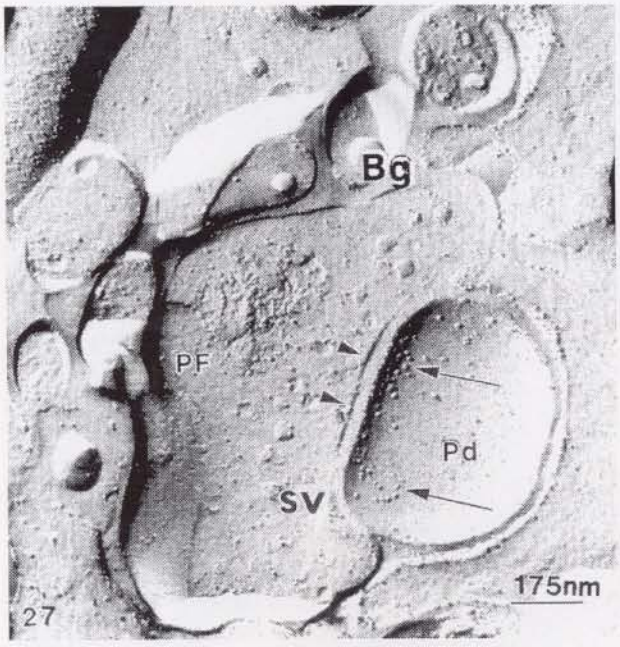

Figure 27. Freeze-etching replica of a mouse parallel fiber-Purkinje spine synaptic contact. The parallel fiber ending (PF) contains spheroidal synaptic vesicles (sv). The arrowheads indicate the presynaptic membrane. The E-face postsynaptic membrane of Purkinje spine (Pd) shows aggregated intramembrane particles (arrows), corresponding to postsynaptic receptors and/or postsynaptic proteins. Note the enveloping Bergmann glial cytoplasm (Bg).

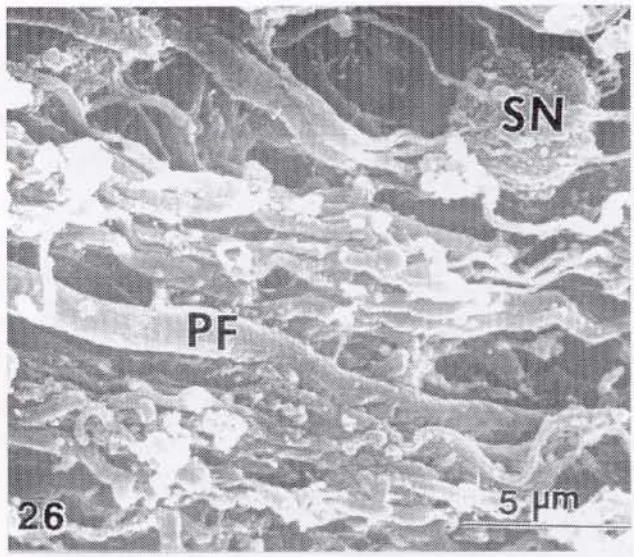

Figure 26. Scanning electron micrograph of a mouse cerebellar molecular layer showing the outer surface of parallel fibers (PF). A stellate neuron (SN) is also seen.

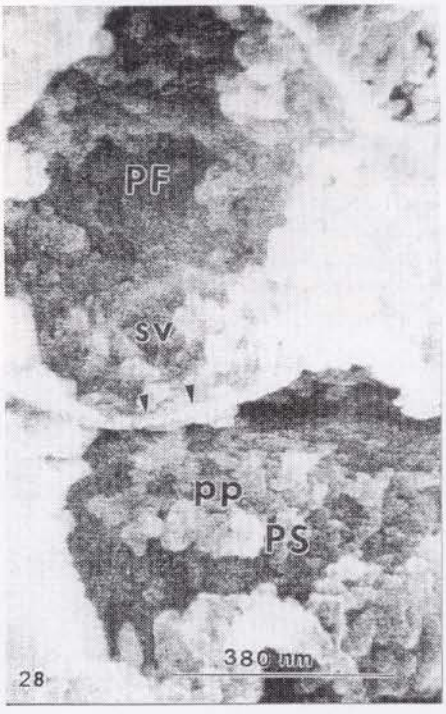

Figure 28. Field emission high resolution scanning electron micrograph of Rhesus monkey molecular layer showing a fracture parallel fiber varicosity (PF) containing spheroidal synaptic vesicles (sv). The arrowheads indicate the SE-I profile of the parallel fiber limiting plasma membrane. The synaptic active site is not resolved. The fractured post-synaptic Purkinje dendritic spine (PS) shows the postsynaptic proteins (pp).

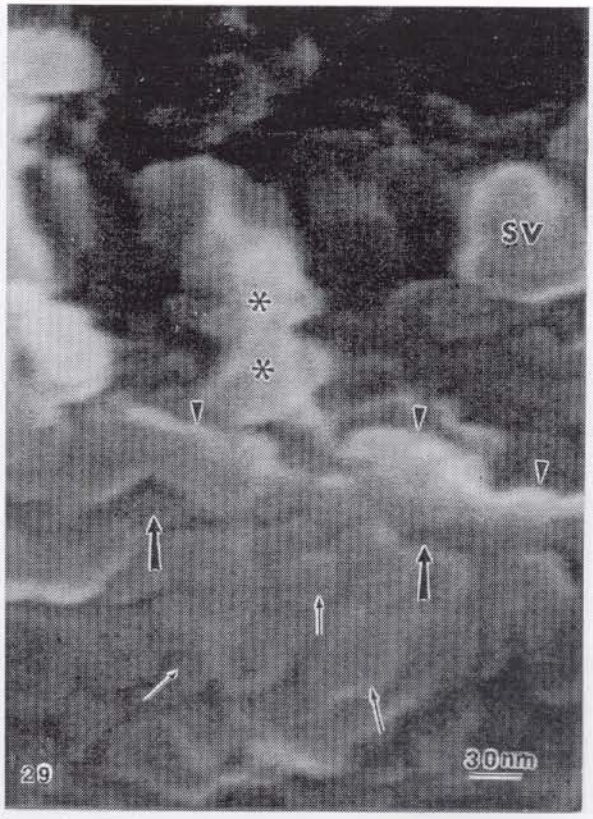

Figure 29. Field emission high resolution scanning electron micrograph showing the parallel fiber-Purkinje spine synaptic membrane contact. The presynaptic dense projection (asterisks) and a synaptic vesicle (sv) are observed in the presynaptic parallel fiber ending. The presynaptic membrane (arrowheads) appears separated from the postsynaptic membrane by the synaptic cleft (thick arrows). The thin arrows label the postsynaptic membrane globular subunit corresponding to the postsynaptic receptors and/or postsynaptic proteins.

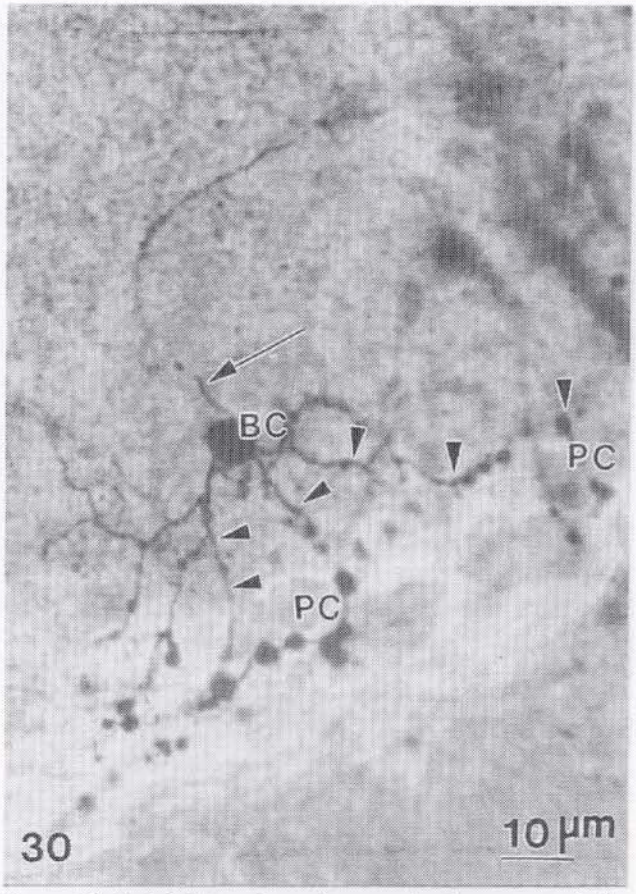

Figure 30. Golgi light photomicrograph of mouse cerebellar basket cell (BC) showing its descending axonal ramifications (arrowheads) toward the Purkinje cells (PC) an ascending basket cell dendrites is also seen (arrow).

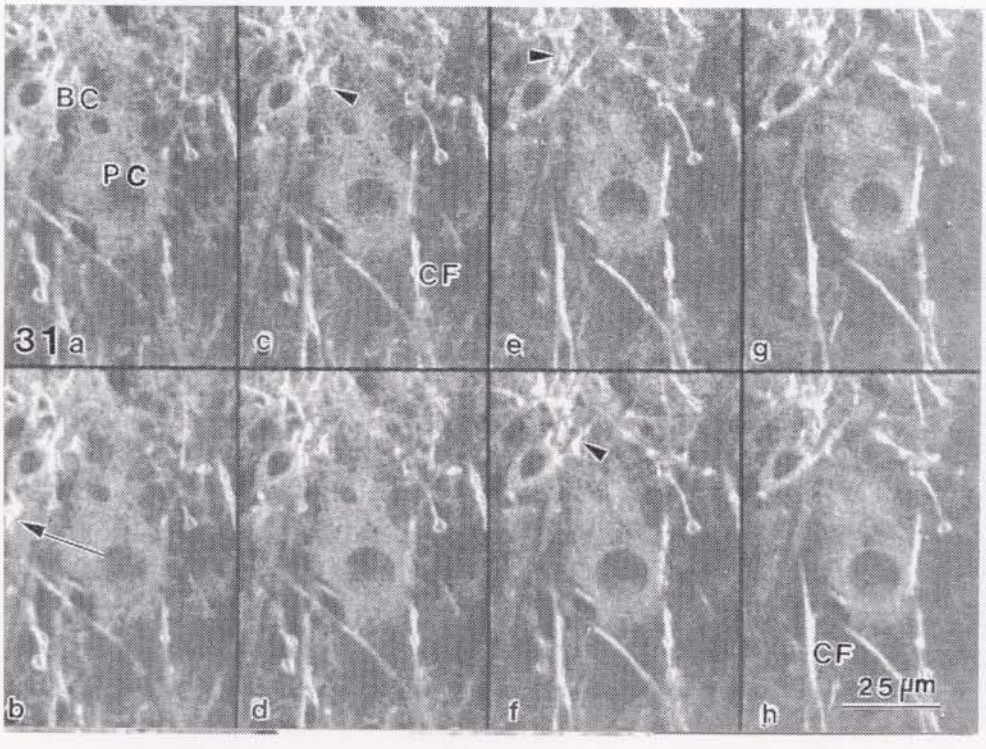

Figure 31 a-h. Z-series of confocal laser scanning microscopy of a basket cell (BC) in close proximity to the upper pole of Purkinje cell (PC) and exhibiting ascending dendrites (arrowheads) and a descending axonal ramification (arrow) toward the Purkinje cell soma. An ascending climbing fiber (CF) is also seen.

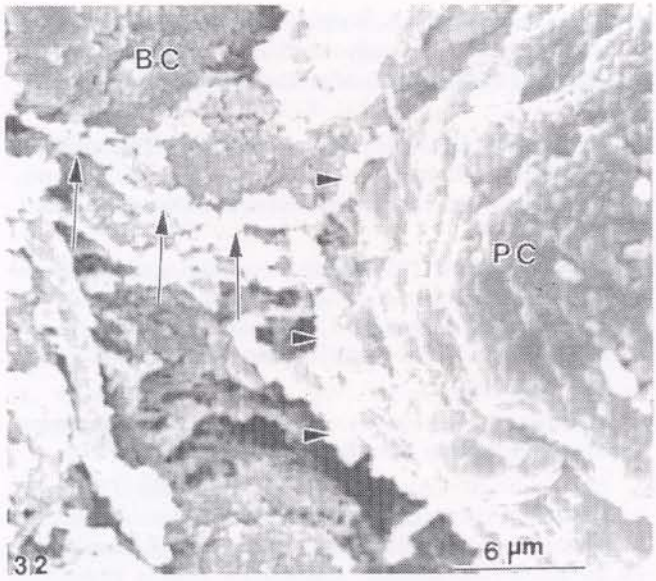

Figure 32. Scanning electron micrograph of human cerebellar basket cell (BC) axonal ramification (arrows) applied (arrowheads) to the Purkinje cell soma (PC) and contributing to the pericellular nest. Ethanol-cryofracturing technique.

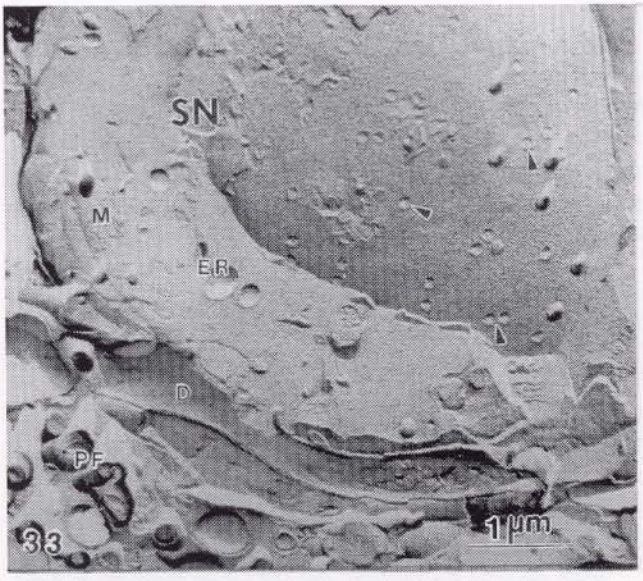

Figure 33. Freeze-etching replica of mouse cerebellar molecular layer showing a fractured stellate neuron (SN). The fracture nuclear envelope exhibits at the P-face of inner nuclear membrane the distribution of intramembrane particles and nuclear pores (arrowheads). The endoplasmic reticulum (ER) and the mitochondria (M) are also seen. The neighbouring molecular layer shows the cross sections of some parallel fibers (PF). A longitudinally fractured dendritic profile (D) is also seen.

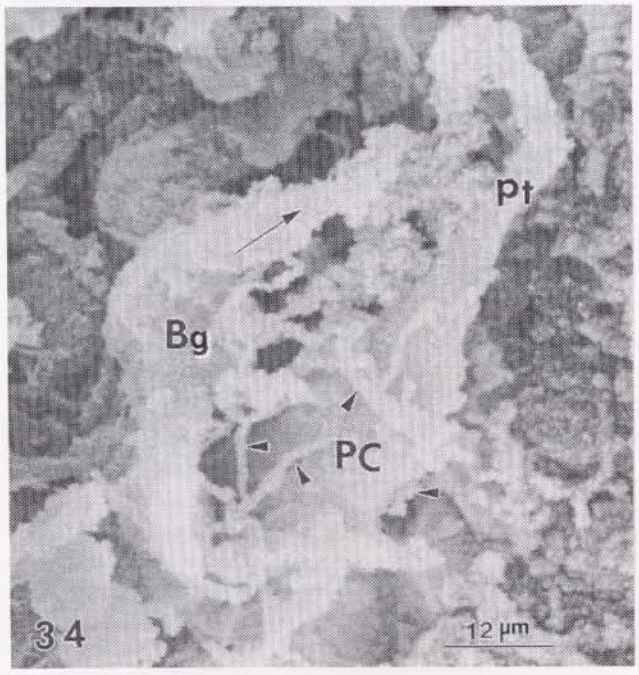

Figure 34. Scanning electron micrograph of the teleost fish Bergmann glial cell outer surface (Bg) surrounding the soma of a Purkinje cell (PC). The Bergmann fiber (arrow) approaches to the Purkinje primary dendritic trunk (pt). A partial view of the Purkinje pericellular nest (arrowheads) is seen.

Figure 35. Freeze-etching replica of mouse cerebellar cortex showing the P-face of Bergmann glial cell plasma membrane showing the overall distribution of intramembrane particles. Note the presence of orthogonal arrays of intramembrane particles (arrowheads).

and climbing fibers in the molecular layer. In freeze-etching replicas, the smooth surface cytoplasm of Bergmann glial cells can be easily traced in the complex neuropil of molecular layer penetrating among the neural structures, which appear as embedded in the Bergmann glial cell cytoplasm. At higher magnification, the smooth surface Bergmann glial cell cytoplasm can be seen surrounding longitudinally exposed isolated parallel fibers or cross-fractured parallel fiber bundles. The Bergmann glial cell encapsulates not only nonsynaptic segments of parallel fibers but also the parallel fiber synaptic varicosities. A novel contribution of freeze-etching replicas for TEM was the visualization of orthogonal arrays of intramembrane particles and elongated rod particles in the P and E faces of Bergmann glial plasma membrane (Fig. 35).

Acknowledgement

This paper have been carried out by a subvention obtained from CONDES-LUZ. The secretary assistanship of Laura Villamizar is deeply appreciated.

References

1. Castejón OJ (1988). Scanning electron microscopy of vertebrate cerebellar cortex. ***Scanning Microsc*** II: 569-597.
2. Ramón y Cajal S (1955). ***Histologie du Système Nerveux de l'Homme et des Vertebres.*** Consejo Superior de Investigaciones Científicas. Instituto Ramón y Cajal, Eds. Vol 2. Madrid. España.
3. Fox CA. (1962). In: ***Correlative Anatomy of the Nervous System. Fine structure of the cerebellar cortex.*** Crosby EC, Humphreys T, Lauer EW, Eds. MacMillan Co New York. USA. pp 192-198.
4. Fox CA, Hillman DE, Siegesmund KA, Dutta CR (1967). The primate cerebellar cortex. A Golgi and electron microscopic study. ***Prog Brain Res*** 25: 174-225.
5. Eccles JC, Ito M, Szentagothai J (1967). ***The Cerebellum as a Neuronal Machine.*** New York: Springer-Verlag.
6. Mugnaini E (1972). The histology and cytology of the cerebellar cortex. In: Larsell O, Jansen J, Eds. ***The Comparative Anatomy and Histology of the Cerebellum. The Human Cerebellum, Cerebellar Connections and Cerebellar Cortex.*** Minneapolis: The University of Minnesota Press. pp 201-264.
7. Palay SL, Chan-Palay V (1974). ***Cerebellar Cortex. Cytology and Organization.*** Berlin: Springer-Verlag.
8. Castejón OJ, Sims P (1999). Confocal laser scanning microscopy of hamster cerebellum using FM4-64 as an intracellular staining. ***Scanning*** 21:15-21.
9. Castejón OJ, Castejón HV (2001). Correlative microscopy of cerebellar granule cells. ***Biocell*** (In Press).
10. Castejón OJ, Caraballo AJ (1980). Light and scanning electron microscopy study of cerebellar cortex of teleost fishes. ***Cell Tissue Res*** 207:211-226.
11. Mugnaini E, Floris A, Wright-Goss M (1994). Extraordinary synapses of the unipolar brush cell: an electron microscopic study in the rat cerebellum. ***Synapse*** 16: 248-311.
12. Mugnaini E, Diño MR; Jaarsma D (1997). The unipolar brush cells of the mammalian cerebellum and cochlear nucleus: cytology and microcircuitry. ***Prog. Brain Res*** 114:131-150.
13. Ramón y Cajal S (1955). Grandes cellules etoilées ou cellules de Golgi. In: ***Histologie du Système Nerveux de l'Homme et des Vertèbres.*** Consejo Superior de Investigaciones Científicas, Instituto Ramón y Cajal, Ed. Vol. 2. Madrid. pp 42-48.
14. Castejón OJ, Castejón HV (2000). Correlative microscopy of cerebellar Golgi cells. ***Biocell*** 24:13-30.
15. Alvarez-Otero R, Anadon R (1992). Golgi cells of the cerebellum of the dogfish, Scyliorhinus canicula (elasmobranch): a Golgi and ultrastructural study. ***J Hirnforschs*** 33: 321-327.
16. Castejón OJ, Castejón HV, Sims P (2000). Confocal, scanning and transmission electron microscopic study of cerebellar mossy fiber glomeruli. ***J Submicrosc Cytol Pathol*** 32:247-260.
17. Fox CA (1959). The intermediate cells of Lugaro in the cerebellar cortex of monkey. ***J. Comp Neurol*** 112:39-51.
18. Laine J, Axelrad H (1996). Morphology of the Golgi-impregnated Lugaro cell in the rat cerebellar cortex: a reappraisal with a description of its axon. ***J Comp Neurol*** 375:618-640.
19. Melik-Musian AB, Fanarjan VV (1998). Structural organization and Lugaro neuron connections in the cat cerebellar cortex. ***Morfologiia*** 113:44-48.
20. Laine J, Axelrad H (1998). Lugaro cells target basket and stellate cells in the cerebellar cortex. ***Neuroreport*** 9:2399-2403.
21. Chan-Palay V (1971). The recurrent collaterals of Purkinje cell axons. A correlated study of the rat's cerebellar cortex with electron microscopy and the Golgi method. ***Z Anat Enwickl Gesch*** 134:200-234.
22. Castejón OJ, Caraballo AJ (1980). Application of cryofracture and SEM to the study of human cerebellar cortex. ***Scanning Electron Microsc*** IV: 197-207.
23. Castejón, OJ, Valero C (1980). Scanning electron microscopy of human cerebellar cortex. ***Cell Tissue Res*** 212:363-374.
24. Scheibel AB, Paul L, Fried I (1981). Scanning electron microscopy of the central nervous system. I The cerebellum. ***Brain Res Rev*** 3:207-228.
25. Hojo T (1994). An experimental scanning electron microscopic study of human cerebellar cortex using t-butil alcohol freeze-drying device. ***Scanning Microsc*** 8:303-313.
26. Arnett CE, Low FN (1985). Ultrasonic microdissection of rat cerebellum for scanning electron microscopy. ***Scanning Electron Microsc*** I: 274-255.
27. Takahashi-Iwanaga H (1992). Reticular endings of Purkinje cell axons in the rat cerebellar nuclei: scanning electron microscopic observations of the pericellular plexus of Cajal. ***Arch Histol Cytol*** 55:307-314.

28. Martonne ME, Zhang Y, Simpliciano VM, Carragher BO, Ellisman M (1993). Three-dimensional visualization of the smooth endoplasmic reticulum in Purkinje cell dendrites. ***J Neurosci*** 13:4636-4646.

29. Terasaki M, Slater NT, Fein A, Schmidek A, Reese TS (1994). Continuous network of endoplasmic reticulum in cerebellar Purkinje neurons. ***Proc Natl Acad Sci USA*** 91:7510-7514.

30. Kanaseki T, Ikeuchi Y, Tashiro Y (1998). Rough surfaced smooth endoplasmic reticulum in rat and mouse cerebellar Purkinje cells visualized by quick-freezing techniques. ***Cell Struct Funct*** 23:373-387.

31. Castejón OJ, Sims P (1999). Cytoarchitectonic arrangement and intracortical circuits of hamster cerebellum. A study by means of confocal laser scanning microscopy. ***Biocell*** 23:187-196.

32. Castejón OJ, Castejón HV, Alvarado MV (2000). Further observations on cerebellar climbing fibers. A study by means of light microscopy, confocal laser scanning microscopy and scanning and transmission electron microscopy. ***Biocell*** 24:197-212.

33. Alvarez-Otero R, Regueira SD, Anadon R (1993). New structural aspects of the synaptic contacts on Purkinje cell in an elasmobranch cerebellum. ***J Anat*** 182:13-21.

34. Castejón OJ, Apkarian RP (1992). Conventional and high resolution scanning electron microscopy of outer and inner surface features of cerebellar nerve cells. ***J Submicrosc Cytol Pathol*** 24:549-562.

35. Castejón OJ, Castejón HV (1997). Conventional and high resolution scanning electron microscopy of cerebellar Purkinje cells. ***Biocell*** 21:149-159.

36. Castejón OJ (1990). Freeze-fracture scanning electron microscopy and comparative freeze-etching study of parallel fiber-Purkinje spine synapses of vertebrate cerebellar cortex. ***J Submicrosc Cytol Pathol*** 22: 281-295.

37. Castejón OJ, Castejón HV, Apkarian RP (1994). High resolution scanning electron microscopy features of primate cerebellar cortex. ***Cell Mol Biol*** 40: 1173-1181.

38. Castejón OJ, Castejón HV, Sims P (2001). Light microscopy, confocal laser scanning microscopy, scanning and transmission electron microscopy of cerebellar basket cells. ***J Submicrosc Cytol Pathol*** 33:1-10.

39. Castejón OJ, Castejón HV (1987). Electron microscopy and glycosaminoglycan histochemistry of cerebellar stellate neurons. ***Scanning Microsc*** 1:681-693.

40. Paula-Barbosa MM, Tavares MA, Ruela C, Barroca H (1983). The distribution of stellate cell descending axons in the rat cerebellum: a Golgi and a combined Golgi-electron microscopical study. ***J. Anat*** 137:757-64.

41. Abbott LC, Sotelo C (2000). Ultrastructural analysis of catecholaminergic innervation in weaver and normal mouse cerebellar cortices. ***J Comp Neurol*** 426:316-329.

42. Kerr WH, Bishop GA (1991). Topographical organization in the origin of serotoninergic projections to different regions of the cat cerebellar cortex. ***J Comp Neurol*** 304:502-515.

43. Castejón OJ (1990). Surface and membrane morphology of Bergmann glial cells and their topographic relationships in the cerebellar molecular layer. ***J Submicrosc Cytol Pathol*** 22: 123-134.